Journal of Engineering Science and Technology
Vol. 17, No. 4 (2022) 2373 - 2389


# DEEP LEARNING-BASED FINE-GRAINED AUTOMATED PNEUMONIA DETECTION MODEL

KEERTHANA RANGASAMY[1], NURUL SHUHADA MOHD FUZI[1], MUHAMMAD AMIR AS'ARI[1,2,*], NUR AZMINA RAHMAD[1], NUR ANIS JASMIN SUFRI[1]

[1]School of Biomedical Engineering and Health Sciences, Faculty of Engineering, Universiti Teknologi Malaysia, Johor Bahru, Malaysia
[2]Sport Innovation and Technology Center (SITC), Institute of Human Centered Engineering (IHCE), Universiti Teknologi Malaysia, Johor Bahru, Malaysia
*Corresponding Author: amir-asari@biomedical.utm.my

## Abstract

Pneumonia is a bacterial, fungal, or viral infection of the lungs that leads the lungs' air sacs to clogged with pus or fluids that are generally diagnosed using chest X-rays (CXR) cost-effective, fast, and non-invasive. However, this diagnosis is complicated by high inter-observer and intra-observer variation among radiologists as it mainly depends on radiologist proficiency. Hence, there is a higher demand for automated, rapid pneumonia detection tools to curb the lack of specialised radiologists, especially in rural areas. Thus, this paper presented a fine-grained deep learning-based automated pneumonia detection system using several well-establish pre-trained Convolutional Neural Network (CNN) models (AlexNet, SqueezeNet, GoogleNet, ResNet-18, and ResNet-50) form CXR images that can be utilised for early diagnosis. The results revealed that all models succeed in detecting pneumonia at an accuracy of over 80%. SquuezeNet outperformed among the other models with an accuracy of 81.62% within a speed of 64.6 minutes.

Keywords: Convolutional neural network, Deep learning, Diagnostic radiography, Medical image processing, Pneumonia detection.

## 1. Introduction

Pneumonia is the predominant cause of death among children in the growing country [1]. World Health Organization (WHO) predicted that one out of three new-born infant death caused by pneumonia [2]. It is also known as an epidemic and chronic disease that costs thousands of lives clearly in this era of the COVID-19 pandemic [3]. It is lung inflammation caused by an infection of bacteria, fungi, or viruses. The inflammation causes the lungs to fill with fluid and affect the pulmonary alveoli, leading to breathing difficulties due to a lack of oxygen circulation throughout the body [4]. The typical pneumonia symptoms are breathing problems, chest pain, fever and chills, confusion, headache, muscle pain, and fatigue [5]. Children, the elderly, and people with weakened immune systems are at the highest risk of suffering pneumonia.

There are several traditional methods employed to diagnose pneumonia through a blood test, pulse oximetry test, sputum culture, and gram stain test, serology, urine antigen test, ultrasound, and chest X-Ray (CXR), CT scan, and MRI. Among these approaches, CXR is widely used to detect pneumonia. However, the interpretation and analysis of these CXR images depend on the radiologist, who is restricted by speed, experience, and fatigue and may be prone to human error [6]. An expert and qualified radiologist costs a substantial financial burden for training, and lower-cost countries lack such radiologists [7]. A fallacious or procrastinated diagnosis may result in casualty [8]. Therefore, an automated Artificial Intelligence (AI) system is essential for rapid pneumonia detection.

With the availability of huge medical imaging data and breakthroughs in current technology, especially in big data and AI, it allows the emergence of deep learning in medical image processing and clinical diagnosis [9]. The deep learning concept has been effectively implemented in numerous health sector applications as automated detection for initial screening processes [10]. Some of these applications are skin cancer classification [11, 12], brain disorder classification [13], arrhythmia identification [14-16], lung segmentation [17, 18], and fundus image segmentation [19]. Hence, these medical breakthroughs from utilising AI technology of deep learning models have inspired developing an automated pneumonia detection system considering the sophisticated, precise, and instant discovery of lung disease.

This paper's main contribution is to propose a fine-grained automated and efficient pneumonia detection system by focusing on dense analysis of comparing well-established pre-trained CNN models which are AlexNet, SqueezeNet, GoogleNet, ResNet-18, and ResNet-50 and their total execution time in classifying between bacterial, viral pneumonia, and normal lung conditions. This CNN algorithm automatically outperforms learning features from input data through a feature learning approach without any human expert feature engineering. The rest of this paper is organised as below in section 2, emphasising literature review; section 3 focuses on methodology, section 4 presents results and discussion, and finally, section 5 conclusion and future direction.

## 2. Background Review

In this section, existing approach for pneumonia detection, in a traditional way as well as deep learning based detection briefed.

## 2.1. Existing approach for pneumonia detection

Traditionally, there are three main methods for pneumonia diagnosis performed by physicians which are physical examination, laboratory tests, and CXR analysis. Table 1 compares these three methods thoroughly. Additionally, as reported by the World Health Organization (WHO), among these approaches, CXR has been the best preference for pneumonia diagnosis [20]. It is a fast and painless imaging test using electromagnetic waves to create images and spot abnormalities of the airways, blood vessels, organs, tissues, and bones. Yet, analysing CXR images for pneumonia detection is a challenging task as it requires expert clinicians in every hospital, which are limited. Thus, there is a substantial need for an automated, rapid pneumonia detection technique.

**Table 1. Existing traditional pneumonia detection approach.**

| Method | | Descriptions / Limitation |
|---|---|---|
| **Physical Examination** | Pulse Oximeter [21] | Low oxygen levels in the blood may mean the person has pneumonia. The presence of pneumonia prevents the lungs from supplying enough oxygen into the bloodstream. / It cannot locate the infected area in the lung. |
| | Stethoscope | Reduced wheezing or crackling sounds in the lungs could be the result of pneumonia./ It cannot locate the infected area in the lung. |
| **Laboratory Tests** | Blood Count Test | Use the blood sample to confirm the infection and identify the type of organism that causes the disease./ Hard to distinguish pneumonia |
| | Serum Procalcitonin test [22] | The serum is a substance produced by cells in the body, often responding to bacterial infections tissue injury. Its level of interest elevated in patients with bacterial pneumonia and septic shock./ Time-consuming and does not classify what type of microorganism is present. |
| | Sputum Culture and Gram Stain Test [23] | A sample of fluid from the lungs (sputum) is taken after a deep cough and analysed to pinpoint the cause of the infection./ Challenging, time-consuming, difficult to grow certain bacteria, such as *Streptococcus* pneumoniae, and culture can produce false-negative results. |
| | Urine Antigen Tests [24] | More accurate than gram stain and sputum culture test./ Urine antigen tests in milder cases of pneumonia are less accurate, and high possibility of misclassification. |
| | Serology [25] | IgM (Immunoglobulin M) antibodies indicate a new infection, while IgG (Immunoglobulin G) antibodies generally indicate that they were infected in the past./ They are challenging to evaluate when sometimes IgM antibodies have been transformed into IgG antibodies. |
| | Polymerase Chain Reaction Test | An alternative to serology screening for typical bacteria. PCR is a test screening for the presence of specific viral or bacterial DNA in the sample./ Results are often available in 1 to 6 hours. It cannot locate the infected area in the lung. |
| | Enzyme Immunoassays Test [26] | These immune tests use antibodies to detect specific viral antigens and can simultaneously screen for multiple viruses. Results can be obtained within 15 minutes to an hour./ Cannot locate the infected area in the lung |
| | Pleural Fluid Culture [27] | A fluid sample is taken by putting a needle between the ribs from the pleural area and analysed to determine the type of infection./ Time-consuming and a higher risk of getting adverse side effects |
| **Medical Imagin** | Ultrasound | Use high-frequency sound waves to look at organs and structures inside the body. It is a fast imaging procedure that has no radiation exposure and more straightforward than other imaging techniques./ The procedure is not standardised for pneumonia detection in the non-peripheral lung. |

| | |
|---|---|
| Chest X-Ray | It can determine the extent and location of the infection./ It cannot determine what kind of germ is causing pneumonia and distinguish the bacterial and viral infections. |
| Computed Tomography (CT) Scan [28] | Recommended if pneumonia is not clearing as quickly as expected. To obtain a more detailed image of the lungs. More accurate than a chest X-Ray./ Not always available in all levels hospital and has limitations of high cost and high doses of radiation |
| Magnetic Resonance Imaging (MRI) | Uses powerful magnets and radio waves to make detailed pictures inside the body. It is not generally used to evaluate pneumonia but may look at the heart, chest vessels, and wall structures. If the lungs are abnormal because of excess fluid, infection, or tumor, MRI may provide additional information about these abnormalities' cause or extent. MRI has no radiation exposure./ Rarely used for the evaluation of pulmonary parenchyma because of the low proton content of the lungs. |
| Bronchoscopy [29] | The thin camera is guided down into the lungs through the nose or mouth. The doctor can thus visualise the inside of the lungs directly. Where necessary, cultures and biopsies can be taken./ Time-consuming and a higher risk of getting adverse side effects. |

## 2.2. Deep learning approach for pneumonia detection

There is a growing trend for deep learning-based detection approach in the medical imaging domain due to the advancement of big data and AI technology [30]. More particularly, CNN yielded promising results in image classification and object detection in various applications, including medical image recognition and analysis [31]. It learns and extracts discriminative features directly from raw input images without any explicit human engineering [31]. CNN has proven to be an effective model class for understanding image content, providing state-of-the-art results on image recognition, segmentation, detection, and retrieval [32]. When trained with adequate regularisation, CNN achieves superior visual object recognition. This network's efficacy in recognising image is one of the main reasons why the world has developed a growing interest in implementing deep learning. Some application of CNN in medical imaging includes diabetic retinopathy disease detection [33], breast cancer detection from ultrasound images [34] and mammographic images [35] and Parkinson's disease early detection from Magnetic Resonance Image (MRI) [36-38]. And lastly, not forgetting its tremendous achievement in pneumonia detection from CXR images. The recent studies on the deep learning-based pneumonia detection model are presented in Table 2. From the literature, it is clear that most of the previous studies on the pneumonia detection model were only focusing on binary classification between normal vs pneumonia infections.

**Table 2. Deep learning-based pneumonia detection approach.**

| Ref, Year | Descriptions |
|---|---|
| **[3], 2020** | Presented binary classification using Deep CNN and succeeded in achieving accuracy of more than 90%. |
| **[39], 2019** | Proposed ensemble of two CNNs, (RetinaNet and Mask R-CNN) for pneumonia detection and localisation and achieve a recall of 0.793. |
| **[40], 2019** | Formulate an 18-layer novel deep sequential CNN based model and attain an accuracy of 0.9439 in classifying normal vs. pneumonia. |
| **[41], 2019** | Designed Xception and Vgg16 based binary classification model network and achieved an accuracy of 0.87% and 0.82%, respectively using 624 frontal chest X-ray images. |

| | |
|---|---|
| **[42], 2018** | Used attention guided two-branch CNN using the ChestX-ray14 dataset for thorax disease classification. The system uses attention heat maps to mask the disease-affected regions used to train the network's local branch. The model achieves an AUC of 0.776. |
| **[43], 2018** | Develop a pre-trained Inception v3 model to classify chest X-rays of binary classification for normal and pneumonia lungs. The model achieved accuracy, sensitivity, specificity of 92.8%, 93.2%, and 90.1%, respectively. |
| **[44], 2017** | Construct a localisation algorithm using 112,120 frontal chests X-rays from the ChestX-ray14 dataset to detect thorax disease and reported to gain area AUC of 0.633. |
| **[45], 2017** | Developed a DenseNet-121 layer with a transfer learning method for binary classification of pneumonia and non-pneumonia classes and achieved 0.60 % AUC value. |
| **[46], 2017** | Established a 121-layer CNN based on DenseNet and named as CheXNet. The network was trained with 10,000 frontal view chest X-ray images with 14 different diseases and achieved AUC of 0.768 and an F1 score of 0.435 (95% CI 0.387, 0.481), higher than the radiologist average of 0.387 (95% CI 0.330, 0.442). |

Besides, the authors in [47], proposed computer aided diagnosis (CAD) system to identify bacterial and viral pneumonia in CXR through lung region identification and pneumonia category classification. AUC value of $0.8234 \pm 0.0014$ was achieved by ensemble AlexNet features with several handcrafted features which are grey level co-concurrence matric features (GLCM) features, Haar wavelet transform features and histogram of oriented gradient (HOG) features. However, the authors only consider AlexNet as pretrained model for one of the classification feature extractions and the classification model seems to be complex where they utilised segmentation with pretrained CNN model as well as several handcrafted features. Moreover, in [48], authors designed pneumonia types of detection model including novel corona virus disease (COVID-19) by only implementing pretrained AlexNet model. Thus, this paper contributes to designing models that classify normal, bacterial, and virus lung infections through dense analysis of comparing several pretrained model (AlexNet, SqueezeNet, GoogleNet, ResNet-18, and ResNet-50) including total execution time for each pretrained models.

## 3. Methods

### 3.1. Project workflow

The flow process of the proposed automated pneumonia detection model is demonstrated in Fig. 1. The methodology starts with dataset selection from CXR Images that can be obtained from Kaggle Datasets, followed by pre-processing of the datasets, development of CNN models using pre-trained CNN, and finally, performance evaluation of the proposed model.

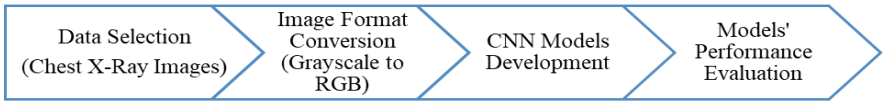


**Fig. 1. Proposed method.**

### 3.2. Dataset selection

In this study, Chest X-Ray (CXR) datasets were obtained from publicly available Kaggle Datasets [49]. These CXR images were selected from paediatric patients of one to five years old from Guangzhou Women and Children's Medical Center, Guangzhou. The CXR images were graded and evaluated by expert physicians before they can be used for training the AI system. A total of 5,856 CXR images were utilised in this study. CXR images' datasets consist of two main categories: normal and pneumonia, and two subcategories of pneumonia, which are bacterial pneumonia and viral pneumonia. The proposed model was designed to detect these three normal categories, bacterial pneumonia and viral pneumonia. These CXR image datasets were then split into training, validation, and testing datasets for training and evaluating the proposed model. Figure 2 shows samples of CXR images.


**Fig. 2. Sample of CXR Image datasets [49].**

### 3.3. Data pre-processing

The chest X-ray (CXR) image datasets from Kaggle Datasets are in grayscale. However, in order to perform transfer learning from pretrained model, the pre-trained CNN network requires input of RGB structure. Hence, to achieve this goal, CXR grayscale image datasets need to mimic RGB structure. So, each one channel grayscale image was replicated to produce three channel RGB structure as desired by input shape of pretrained CNN model [50].

### 3.4. Transfer learning using pretrained model

The pneumonia detection model was developed using five different pre-trained CNN models that include AlexNet [51], SqueezeNet [52], GoogleNet [53], ResNet-18 [54], and ResNet-50 [55] to study its performance level in detecting pneumonia. This pre-trained CNN models' architecture is distinct from one another in terms of depth, size, and image input size. The input size of CNN model was chosen as predefined by each pretrained model. The properties of the CNN model are tabulated in Table 3. The architectures of these five pretrained CNN model are presented below.

**Table 3. Properties of CNN model [56].**

| Model | Network | Depth | Size (MB) | Input Size |
|---|---|---|---|---|
| **1** | AlexNet | 8 | 227 | 227×227 |
| **2** | SqueezeNet | 18 | 4.6 | 227×227 |
| **3** | GoogleNet | 22 | 27 | 224×224 |
| **4** | ResNet-18 | 18 | 44 | 224×224 |
| **5** | ResNet-50 | 50 | 96 | 224×224 |

### 3.4.1. AlexNet

AlexNet pretrained CNN model is similar to LeNet, yet deeper. To incorporate non-linear properties, it has Rectifies Linear Unit (ReLU) as a replacement of Tanh function in LeNet. It has dropouts layer for regularization to overcome overfitting issues. To reduce the size of the network, overlapping pooling was utilised. It has five convolutional layers and pooling layers, and it takes and input shape of 227×227×3. The last fc3 fully connected layer and softmax layer were fine-tuned with CXR datasets.

### 3.4.2. SqeezeNet

SqeezeNet CNN model architecture have several refinements in order to reduce the number of parameters yet achieve high accuracy [57]. It replaces 3×3 convolutional filters with 1×1 filters. It decreases the number of input channel to 3×3. It encompasses large activation maps with delayed downsampling implementation. It has several fire modules where a squeeze convolutional layer with 1×1 filters passing into an expand layer that contains a mixture of 1×1 and 3×3 convolution filters. In short, it has 2 convolutional layers, 8 fire module, 4 pooling layers. In takes input image size of 227×227×3. And the last two dense layer of SqeezeNet (convolutional and softmax layer) were fine-tuned with CXR datasets.

### 3.4.3. GoogleNet

The architecture of GoogleNet is 22 layers deep, 27 with pooling layers include [58]. It mainly constructed from 9 inception modules. This model has 3 convolutional layers, 4 maximum pooling layers, an average pooling layer. It has parallel convolution instead of fully connected layers. To reduce the number of inputs the module has 1×1 convolutional layers at the bottom. The last two dense layers were fine-tuned for CXR datasets.

### 3.4.4. ResNet-18

ResNet-18 model has residual learning framework of 18-layers deep. Residual framework means skipping of convolutional layers by using shortcut connections. It has 16 convolutional layers, two downsampling layers and one fully connected layer [59]. It takes inputs in a size of 224×224. The last two dense layer of ResNet-18 was fine-tuned for CXR datasets.

### 3.4.5. ResNet-50

Similar to ResNet-18, ResNet-50 also has residual learning framework. It is 50 layers deep. It has 48 convolutional layers, a max pooling layer, an average pooling layer and a fully connected layer [60]. It takes inputs in a shape of 224×224. And the last two dense layers of ResNet-50 was fine-tuned for CXR datasets.

## 3.5. Proposed pneumonia detection model

As aforementioned, a total of 5,856 CXR images were used in this study. The dataset was first split into 90% of training datasets and 10% testing datasets from these images. Then from 90% of the training datasets, it's further subdivided into 30% validation datasets, which means 90% of datasets were subdivided into 70% training datasets and 30% validation datasets training and validation process. The

datasets were resized into each CNN model's required input shape before passing them into the model. AlexNet and SqueezeNet input size were set to 227×227×3 while GoogleNet, ResNet-50 and ResNet-18 were specified to 224×224×3.

The pneumonia detection model developed using a transfer learning approach where only the last two dense layers had fine-tuned with the CXR datasets. From the input datasets, these CNN models extract global-level image features from the normal, bacterial pneumonia, and viral pneumonia of CXR datasets by learning low-level features to high-level features through spatial relationships from the first layers to the deep last layers, including edge, corner, shape, colour and textural attributes.

The output obtained from the highest probability of the CNN model's final softmax layer detected the normal or pneumonia lung. The CXR datasets were trained using training datasets and validated using validation datasets using five different CNN models. Figure 3 shows proposed pneumonia detection model using one of the pretrained CNN model (SqueezeNet).

The training process was repeated for five-time, and the average score for accuracy was obtained. Throughout these experiments, the batch size set to 10, the epoch set to 6, and the learning rate set to 3e-4. After training, the fine-tuned models were evaluated using test datasets. The performance of the models' accuracy was presented in terms of the confusion matrix. From the obtained accuracy, the performance of these five pre-trained models was evaluated. This entire study was implemented using MATLAB 2018b software.

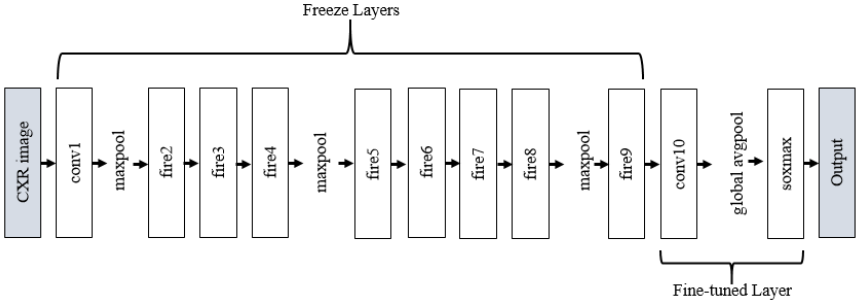


**Fig. 3. Pneumonia detection model using pretrained SqueezeNet.**

## 3.6. Model performance evaluation

Model performance was evaluated using test dataset. Pneumonia detection model was repeated five times for each pretrained model to obtained average accuracy. Accuracy defined as the ratio of correctly classified images over the total images. And the average accuracy is calculated by dividing the obtained 5 accuracies by 5.

The model performance also was evaluated through time taken to complete each testing. Since the experiment is repeated five time for each pretrained model, the time taken to complete each execution also averaged. The average accuracy and average time taken to complete each execution is presented in Table 4. Besides, model's performance also displayed in terms of confusion matrix for clearer understanding which is based on true positive (TP), true negative (TN), false positive (FP), and false negative (FN).

**Table 4. Model performance of proposed pre-trained CNN models.**

| No. | Model | Accuracy (%) | Average (%) | Duration (Minutes) | Average (Minutes) |
|---|---|---|---|---|---|
| **1** | AlexNet | 80.15 | | 62 | |
| | | 81.00 | | 61 | |
| | | 80.66 | 80.80 | 89 | 72.2 |
| | | 81.42 | | 74 | |
| | | 80.78 | | 75 | |
| **2** | SqueezeNet | 81.48 | | 56 | |
| | | 80.15 | | 64 | |
| | | 83.06 | 81.62 | 68 | 64.6 |
| | | 81.23 | | 65 | |
| | | 82.17 | | 70 | |
| **3** | GoogleNet | 79.9 | | 100 | |
| | | 82.05 | | 90 | |
| | | 81.42 | 81.37 | 114 | 106.6 |
| | | 81.42 | | 115 | |
| | | 82.05 | | 114 | |
| **4** | ResNet-18 | 80.58 | | 84 | |
| | | 79.46 | | 108 | |
| | | 81.23 | 80.47 | 109 | 102.4 |
| | | 81.04 | | 107 | |
| | | 80.03 | | 104 | |
| **5** | ResNet-50 | 82.49 | | 223 | |
| | | 79.60 | | 228 | |
| | | 78.40 | 80.60 | 250 | 262.0 |
| | | 80.34 | | 299 | |
| | | 82.17 | | 310 | |

To present the performance of models in view of confusion matrix, the highest accuracy among five repetitions were chosen and the accuracy matrix which are precision, recall, F1-score that represented by confusion matrix also presented in Table 5. Precision is the proportionality of correctly predicted positive image classes to the total predicted positive image classes. Recall is the proportionality of correctly predicted positive image classes to all image classes in actual classes. And F1 score is the weighted average of recall and precision. Since f1 score takes both precision and recall into account, the f1 score is used as parameter for model accuracy evaluation.

**Table 5. Accuracy matrix of proposed pre-trained CNN models.**

| Model | Class | Precision | Recall | F1-Score | Accuracy |
|---|---|---|---|---|---|
| **1** | Normal | 0.943 | 0.930 | 0.936 | |
| | B.Pneumonia | 0.825 | 0.838 | 0.831 | **81.4%** |
| | V.Pneumonia | 0.656 | 0.648 | 0.652 | |
| **2** | Normal | 0.874 | 0.960 | 0.915 | |
| | B.Pneumonia | 0.855 | 0.858 | 0.856 | **83.1%** |
| | V.Pneumonia | 0.721 | 0.643 | 0.680 | |
| **3** | Normal | 0.962 | 0.937 | 0.949 | |
| | B.Pneumonia | 0.791 | 0.889 | 0.837 | **82.0%** |
| | V.Pneumonia | 0.713 | 0.568 | 0.632 | |
| **4** | Normal | 0.961 | 0.914 | 0.937 | |
| | B.Pneumonia | 0.777 | 0.893 | 0.831 | **81.2%** |
| | V.Pneumonia | 0.717 | 0.553 | 0.624 | |
| **5** | Normal | 0.928 | 0.963 | 0.945 | |
| | B.Pneumonia | 0.834 | 0.844 | 0.839 | **82.5%** |
| | V.Pneumonia | 0.685 | 0.643 | 0.663 | |

## 4. Results and Analysis

As aforementioned, this study was conducted to detect pneumonia in the chest by developing a model to classify normal, bacterial, and viral pneumonia lung from CXR datasets attained from free publicly available Kaggle Datasets. This experiment was performed using five different pre-trained CNN models to identify the best pre-trained pneumonia detection, model. Only the last two dense layers from the CNN model were fine-tuned and retrained with the CXR datasets. And from the five repetition results from these five pretrained CNN models, the model with highest accuracy were presented in the form of a confusion matrix in Fig. 4. The precision, recall, and F1 score are tabulated in Table 5. Besides, the average accuracy of each model after five repetitions together with total time of execution is shown in Table 4.

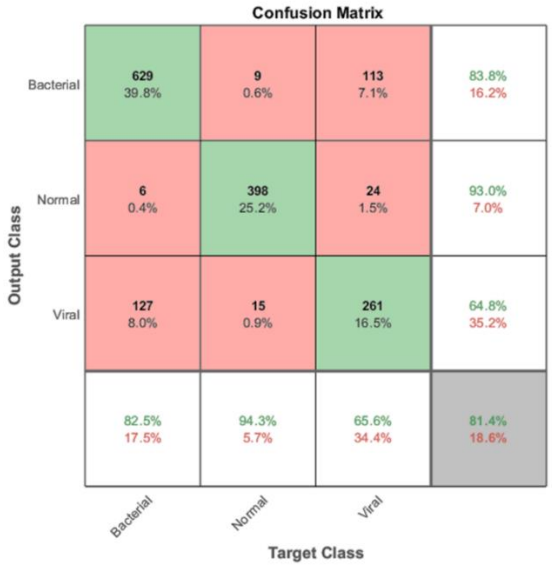


**(a)**

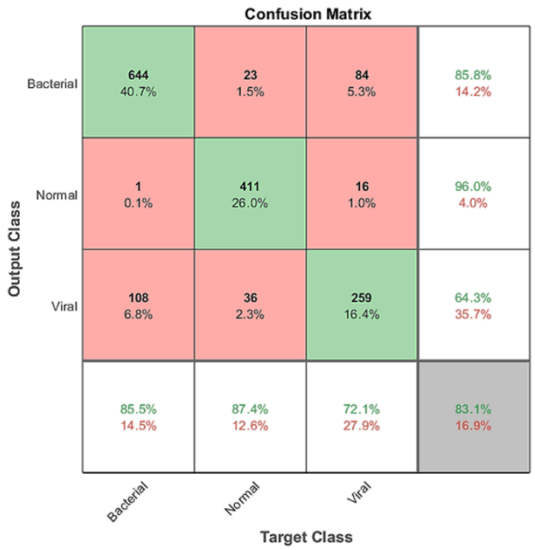


**(b)**


**(c)**


**(d)**

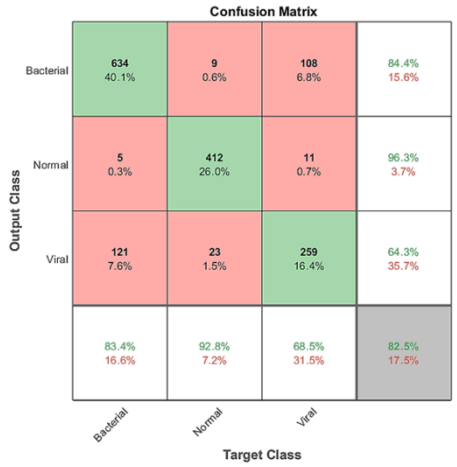


**(e)**

**Fig. 4. The confusion matrix of five different models of (a) AlexNet, (b) SqueezeNet (c)GoogleNet, (d)ResNet-18 and (e)ResNet-50.**

Table 5 illustrates that all the five models outperformed in pneumonia detection as their accuracy above 80%, from Fig. 4. Among these five models, SqeezeNet model accuracy was the highest, 81.6%, followed by GoggleNet, AlexNet, ResNet-50, and ResNet-18. These models' accuracies indicate that model accuracy is not merely dependent on model depth itself.

In terms of classification or pneumonia detection accuracy, from Fig. 4. and f1 score of Table 5 reveals that all the models can accurately be distinguished from normal or healthy lung with pneumonia lung conditions. The f1-score of each pretrained model to identify healthy lung (normal lung condition) was the highest in which all achieve accuracy above 90% where AlexNet (93.6%) , SqueezeNet (91.5%), GoogleNet (94.9%), ResNet-18 (93.7%) and ResNet-50 (94.5%).

In recognizing bacterial pneumonia lung condition, these models' accuracies were in fairly acceptable range where all models achieve f1-score more than 80%; AlexNet (83.1%), SqueezeNet (85.6%), GoogleNet (83.7%), ResNet-18 (83.2%) and ResNet-50 (83.9%). However, in categorizing viral pneumonia lung conditions, the performance of these models dropped where f1-score of these models were in range of 60% above. AlexNet (65.2%), SqueezeNet (68.0%), GoogleNet (63.2%), ResNet-18 (62.4%) and ResNet-50 (66.3%). There are some confusions between both viral and bacterial pneumonia as both images shared almost similar features that have cloudiness in the lung area. The region of the normal healthy lung is non-cloudy, and the edges are to be seen compared to unhealthy pneumonia lung, which is covered with haze.

The model efficiency was measured using time taken to complete each pretrained model execution (average time for five repetition) as presented in Table 4. Among these five pretrained model SqueezeNet achieve fastest execution time where it takes only around 64.6 minutes to complete followed by AlexNet (72.2 minutes), ResNet-18 (102.4 minutes), GoogleNet (106.6 minutes) and ResNet-50 (262.0 minutes).

As these proposed models outperformed in distinguishing between healthy lungs and pneumonia infected lungs with highest accuracy of more 90% at fastest rate hence, these models can be utilised for early, rapid detection between normal and abnormal lung conditions indicating pneumonia. Patients diagnosed with pneumonia can immediately be sent for further treatment without any delay to prevent any mishap. However, in determining between bacterial pneumonia with viral pneumonia these models are quite imprecise, as the models slightly mixed up although it achieves fairly acceptable accuracy of more than 80% in recognizing bacterial pneumonia.

## 5. Conclusions

In this study, fine-grained deep learning-based transfer learning CNN models were proposed on pneumonia detection in CXR images. The proposed automated system can recognise normal, bacterial pneumonia, and viral pneumonia from the CXR images with comparable accuracy. Although in this current COVID-19 pandemic, there are quite a number of papers were extended their study to COVID-19 detection, yet COVID-19 detection is not within the scope of this paper. These results provide compelling evidence that this system facilitated faster pneumonia detection. The results were encouraging, and future studies should be validated on various ages,

including adults and the elderly. Future work should also focus on COVID-19 recognition and develop a hybrid model to enhance feature extraction and improve the model's performance by enhancing each class accuracy higher than 95.0%.

## Acknowledgements

The authors would like to express their gratitude to Universiti Teknologi Malaysia (UTM) for supporting this research and Ministry of Higher Education under Fundamental Research Grant Scheme (FRGS/1/2018/ICT02/UTM/02/9).

## References

1. Angeline, R.; Mrithika, M.; Raman, R.; and Warrier, P. (2020). Pneumonia Detection and Classification Using Chest X-Ray Images with Convolutional Neural Network. *International Conference on Computational Vision and Bio Inspired Computing*. Springer, 701-709.
2. Aponte, J. et al. (2018). MCEE-WHO ill. Retrieved October 20, 2020, from http://www.who.int/healthinfo/global_burden_disease/en/.
3. El Asnaoui, K.; Chawki, Y.; and Idri, A. (2021). Automated Methods for Detection and Classification Pneumonia based on X-Ray Images Using Deep Learning. *Artificial Intelligence and Blockchain for Future Cybersecurity Applications*. Springer, Cham, 257-284
4. Pneumonia NHLBI, NIH. Retrieved October 20, 2020, from https://www.nhlbi.nih.gov/health-topics/pneumonia.
5. Scotta, M.C.; Marostica, P.J.C.; and Stein, R.T. (2019). Pneumonia in Children. *Kendig's Disorders of the Respiratory Tract in Children*. Elsevier, 427-438.
6. Razzak, M.I.; Naz, S.; and Zaib, A. (2018). Deep learning for medical image processing: Overview, challenges and the future. *Classification in BioApps*. 323-350.
7. Yadav, S.S.; and Jadhav, S.M. (2019). Deep convolutional neural network based medical image classification for disease diagnosis. *Journal of Big Data*, 6(1), 1-18.
8. Ker, J.; Wang, L.; Rao, J.; and Lim, T. (2017). Deep learning applications in medical image analysis. *IEEE Access*, 6, 9375-9389.
9. Anwar, S.M.; Majid, M.; Qayyum, A.; Awais, M.; Alnowami, M.; and Khan, M.K. (2018). Medical image analysis using convolutional neural networks: A review. *Journal of Medical Systems*, 42(11), 1-13.
10. Ozturk, T.; Talo, M.; Yildirim, E.A; Baloglu, U.B.; Yildirim, O.; and Acharya, U.R. (2020). Automated detection of COVID-19 cases using deep neural networks with X-ray images. *Computers in Biology and Medicine*, 121, 103792.
11. Esteva.; A Kuprel, B.; Novoa, R.A.; Ko, J.; Swetter, S.M.; Blau, H.M.; and Thrun, S. (2017). Dermatologist-level classification of skin cancer with deep neural networks. *Nature*, 542(7639), 115-118.
12. Codella, N.C.F.; Nguyen, Q.B.; Pankanti, S.; Gutman, D.A.; Helba, B.; Halpern, A.C. and Smith, J.R. (2017). Deep learning ensembles for melanoma recognition in dermoscopy images. *IBM Journal of Research and Development*, 61(4/5), 5-1.

13. Talo, M.; Yildirim, O.; Baloglu, U.B.; Aydin, G.; and Acharya, U.R. (2019). Convolutional neural networks for multi-class brain disease detection using MRI images. *Computerized Medical Imaging and Graphics*, 78, 101673.
14. Yıldırım, Ö.; Pławiak, P.; Tan, R.S.; and Acharya, U.R. (2018). Arrhythmia detection using deep convolutional neural network with long duration ECG signals. *Computers in biology and medicine*, 102, 411-420.
15. Hannun, A.Y.; Rajpurkar, P.; Haghpanahi, M.; Tison, G.H.; Bourn, C.; Turakhia, M.P.; and Ng, A.Y. (2019). Cardiologist-level arrhythmia detection and classification in ambulatory electrocardiograms using a deep neural network. *Nature medicine*, 25(1), 65-69.
16. Acharya, U.R.; Oh, S.L.; Hagiwara, Y.; Tan, J.H.; Adam, M.; Gertych, A.; and San Tan, R. (2017). A deep convolutional neural network model to classify heartbeats. *Computers in biology and medicine*, 89, 389-396.
17. Gaál, G.; Maga, B.; and Lukács, A. (2020). Attention u-net based adversarial architectures for chest x-ray lung segmentation. *arXiv preprint arXiv:*2003.10304.
18. Souza, J.C.; Diniz, J.O.B.; Ferreira, J.L.; da Silva, G.L.F.; Silva, A.C.; and de Paiva, A.C. (2019). An automatic method for lung segmentation and reconstruction in chest X-ray using deep neural networks. *Computer methods and programs in biomedicine*, 177, 285-296.
19. Tan, J.H.; Fujita, H.; Sivaprasad, S.; Bhandary, S.V.; Rao, A.K.; Chua, K.C.; and Acharya, U.R. (2017). Automated segmentation of exudates, haemorrhages, microaneurysms using single convolutional neural network. *Information sciences*, 420, 66-76.
20. Cherian, T.; Mulholland, E.K.; Carlin, J.B.; Ostensen, H.; Amin, R.; Campo, M.D.; Greenberg, D.; Lagos, R.; Lucero, M.; Madhi, S.A. and O'Brien, K.L. (2005). Standardized interpretation of paediatric chest radiographs for the diagnosis of pneumonia in epidemiological studies. *Bulletin of the World Health Organization*, 83, 353-359.
21. Levin, K.P.; Hanusa, B.H.; Rotondi, A.; Singer, D.E.; Coley, C.M.; Marrie, T.J.; Kapoor, W.N.; and Fine, M.J. (2001). Arterial blood gas and pulse oximetry in initial management of patients with community-acquired pneumonia. *Journal of General Internal Medicine*, 16(9), 590-598.
22. Simon, L.; Gauvin, F.; Amre, D.K.; Saint-Louis, P.; and Lacroix, J. (2004). Serum procalcitonin and C-reactive protein levels as markers of bacterial infection: a systematic review and meta-analysis. *Clinical Infectious Diseases*, 39(2), 206-217.
23. Jonas, V.; Alden, M.J.; Curry, J.I.; Kamisango, K.; Knott, C.A.; Lankford, R.; Wolfe, J.M.; and Moore, D.F. (1993). Detection and identification of Mycobacterium tuberculosis directly from sputum sediments by amplification of rRNA. *Journal of Clinical Microbiology*, 31(9), 2410-2416.
24. Murdoch, D.R.; Laing, R.T.; Mills, G.D.; Karalus, N.C.; Town, G.I.; Mirrett, S.; and Reller, L.B. (2001). Evaluation of a rapid immunochromatographic test for detection of Streptococcus pneumoniae antigen in urine samples from adults with community-acquired pneumonia. *Journal of Clinical Microbiology*, 39(10), 3495-3498..

25. Vincent, A.; La Scola, B.; Forel, J.M.; Pauly, V.; Raoult, D.; and Papazian, L. (2009). Clinical significance of a positive serology for mimivirus in patients presenting a suspicion of ventilator-associated pneumonia. *Critical Care Medicine*, 37(1), 111-118.
26. Kazandjian, D.; Chiew, R.; and Gilbert, G.L. (1997). Rapid diagnosis of Legionella pneumophila serogroup 1 infection with the Binax enzyme immunoassay urinary antigen test. *Journal of Clinical Microbiology*, 35(4), 954-956.
27. Modern Weng, D.O.; and Case Lo, C. (2017) Pleural Fluid Culture. Retrieved October 20, 2020, from https://www.healthline.com/health/pleural-fluid-culture.
28. Hayden, G.E.; and Wrenn, K.W. (2009). Chest radiograph vs. computed tomography scan in the evaluation for pneumonia. *The Journal of Emergency Medicine*, 36(3), 266-270.
29. Bliggers, A. and Leonard, J. (2018). What to expect from a bronchoscopy. Retrieved October 20, 2020, from https://www.medicalnewstoday.com/articles/322178.
30. Suzuki, K. (2017). Overview of deep learning in medical imaging. *Radiological Physics and Technology*, 10(3), 257-273.
31. Lundervold, A.S.; and Lundervold, A. (2019). An overview of deep learning in medical imaging focusing on MRI. *Zeitschrift für Medizinische Physik*, 29(2), 102-127.
32. Aloysius, N.; and Geetha, M. (2017). April. A review on deep convolutional neural networks. In 2017 *International Conference on Communication and Signal Processing* (*ICCSP*), 0588-0592.
33. Jia, X.; and Meng, M.Q.H. (2016). A deep convolutional neural network for bleeding detection in wireless capsule endoscopy images. In 2016 38*th Annual International Conference of the IEEE Engineering in Medicine and Biology Society* (*EMBC*), 639-642
34. Yuan, Y.; and Meng, M.Q.H. (2017). Deep learning for polyp recognition in wireless capsule endoscopy images. *Medical Physics*, 44(4), 1379-1389.
35. Xie, W.; Noble, J.A.; and Zisserman, A. (2018). Microscopy cell counting and detection with fully convolutional regression networks. *Computer Methods in Biomechanics and Biomedical Engineering: Imaging & Visualization*, 6(3), 283-292.
36. Mak, E.; Su, L.; Williams, G.B.; Firbank, M.J.; Lawson, R.A.; Yarnall, A.J.; Duncan, G.W.; Mollenhauer, B.; Owen, A.M.; Khoo, T.K.; and Brooks, D.J. (2017). Longitudinal whole-brain atrophy and ventricular enlargement in nondemented Parkinson's disease. *Neurobiology of Aging*, 55, 78-90.
37. Hopes, L.; Grolez, G.; Moreau, C.; Lopes, R.; Ryckewaert, G.; Carrière, N.; Auger, F.; Laloux, C.; Petrault, M.; Devedjian, J.C.; and Bordet, R. (2016). Magnetic resonance imaging features of the nigrostriatal system: biomarkers of Parkinson's disease stages?. *PLoS One*, 11(4), e0147947.
38. Sivaranjini, S.; and Sujatha, C.M. (2020). Deep learning based diagnosis of Parkinson's disease using convolutional neural network. *Multimedia Tools and Applications*, 79(21), 15467-15479.
39. Sirazitdinov, I.; Kholiavchenko, M.; Mustafaev, T.; Yixuan, Y.; Kuleev, R.; and Ibragimov, B. (2019). Deep neural network ensemble for pneumonia

localization from a large-scale chest x-ray database. *Computers & Electrical Engineering*, 78, 388-399.

40. Siddiqi, R. (2019). Automated pneumonia diagnosis using a customized sequential convolutional neural network. In *Proceedings of the* 2019 3*rd International Conference on Deep Learning Technologies*. 64-70.
41. Ayan, E.; and Ünver, H.M. (2019). Diagnosis of pneumonia from chest X-ray images using deep learning. In 2019 *Scientific Meeting on Electrical-Electronics & Biomedical Engineering and Computer Science* (*EBBT*). IEEE, 1-5.
42. Guan, Q.; Huang, Y.; Zhong, Z.; Zheng, Z.; Zheng, L.; and Yang, Y. (2018). Diagnose like a radiologist: Attention guided convolutional neural network for thorax disease classification. *arXiv preprint arXiv:*1801.09927.
43. Kermany, D.S.; Goldbaum, M.; Cai, W.; Valentim, C.C.; Liang, H.; Baxter, S.L.; McKeown, A.; Yang, G.; Wu, X.; Yan, F.; and Dong, J. (2018). Identifying medical diagnoses and treatable diseases by image-based deep learning. *Cell*, 172(5), 1122-1131.
44. Wang, X.; Peng, Y.; Lu, L.; Lu, Z.; Bagheri, M.; and Summers, R.M. (2017). Chestx-ray8: Hospital-scale chest x-ray database and benchmarks on weakly-supervised classification and localization of common thorax diseases. In *Proceedings of The IEEE Conference on Computer Vision and Pattern Recognition*, 2097-2106.
45. Antin, B.; Kravitz, J.; and Martayan, E. (2017). Detecting pneumonia in chest X-Rays with supervised learning. *Semanticscholar. org*.
46. Rajpurkar, P.; Irvin, J.; Zhu, K.; Yang, B.; Mehta, H.; Duan, T.; Ding, D.; Bagul, A.; Langlotz, C.; Shpanskaya, K.; and Lungren, M.P. (2017). Chexnet: Radiologist-level pneumonia detection on chest x-rays with deep learning. *arXiv preprint arXiv:*1711.05225.
47. Gu, X.; Pan, L.; Liang, H.; and Yang, R. (2018). Classification of bacterial and viral childhood pneumonia using deep learning in chest radiography. In *Proceedings of the* 3*rd International Conference on Multimedia and Image Processing*, 88-93.
48. Ibrahim, A.U.; Ozsoz, M.; Serte, S.; Al-Turjman, F.; and Yakoi, P.S. (2021). Pneumonia classification using deep learning from chest X-ray images during COVID-19. *Cognitive Computation*, 1-13.
49. Mooney, P. (2018). Chest X-Ray Images (Pneumonia) | Kaggle. Retrieved October 20, 2020, from https://www.kaggle.com/paultimothymooney/chest-xray-pneumonia.
50. Xie, Y.; and Richmond, D. (2018). Pre-training on grayscale imagenet improves medical image classification. In *Proceedings of the European Conference on Computer Vision* (*ECCV*) *Workshops*. 0-0.
51. Krizhevsky, A.; Sutskever, I.; and Hinton, G.E. (2017). ImageNet classification with deep convolutional neural networks. *Communications of the ACM*, 60(6), 84-90.
52. Iandola, F.N.; Han, S.; Moskewicz, M.W.; Ashraf, K.; Dally, W.J.; and Keutzer, K. (2016). SqueezeNet: AlexNet-level accuracy with 50× fewer parameters and< 0.5 MB model size. *arXiv preprint arXiv:*1602.07360.

53. Szegedy, C.; Liu, W.; Jia, Y.; Sermanet, P.; Reed, S.; Anguelov, D.; Erhan, D.; Vanhoucke, V.; and Rabinovich, A. (2014). Going deeper with convolutions. *arXiv* 2014, *arXiv:*1409.4842.
54. He, K.; Zhang, X.; Ren, S.; and Sun, J. (2016). Deep residual learning for image recognition. In Proceedings *of the IEEE Conference on Computer Vision and Pattern Recognition*. 770-778.
55. K. He, X. Zhang, S. Ren and J. Sun, (2016). Deep residual learning for image recognition. *Proceedings of the IEEE Conference on Computer Vision and Pattern Recognition*, 770-778.
56. Pretrained Deep Neural Networks - MATLAB & Simulink. Retrieved May 26, 2021, from https://www.mathworks.com/help/deeplearning/ug/pretrained-convolutional-neural-networks.html.
57. Lee, H.J.; Ullah, I.; Wan, W.; Gao, Y.; and Fang, Z. (2019). Real-time vehicle make and model recognition with the residual SqueezeNet architecture. *Sensors*, 19(5), 982.
58. Zhong, Z.; Jin, L.; and Xie, Z. (2015). High performance offline handwritten Chinese character recognition using GoogLenet and directional feature maps. In 2015 13*th International Conference on Document Analysis and Recognition* (*ICDAR*), 846-850
59. Ou, X.; Yan, P.; Zhang, Y.; Tu, B.; Zhang, G.; Wu, J.; and Li, W. (2019). Moving object detection method via ResNet-18 with encoder-decoder structure in complex scenes. *IEEE Access*, 7, 108152-108160.
60. Çinar, A.; and Yildirim, M. (2020). Detection of tumors on brain MRI images using the hybrid convolutional neural network architecture. *Medical Hypotheses*, 139, 109684.